Sulfidation Mechanism and Hydrogenation Activity Regulation of Iron Oxides Sulfurized with Elemental Sulfur for Coal Liquefaction Catalysts

Yahui Yao [a, b, #], *Yang Bai* [c, #], *Lei Tian* [d], *Qiang Guo* [d, *], *Jianfeng Hu* [a, b, *]

Yong Yang [d, *], *Hao Zhang* [a, b, *]

[a] College of Chemistry & Chemical Engineering, Inner Mongolia University, Hohhot, 010021, China

[b] Inner Mongolia Key Laboratory of Synthesis and Application of Organic Functional 10 Molecules, Inner Mongolia University, Hohhot 010021, China

[c] Tianjin Key Laboratory of Applied Catalysis Science and Technology, School of Chemical Engineering, Tianjin University, Tianjin 300350, China

[d] National Energy Center for Coal to Liquids, Synfuels China Co., Ltd, Beijing, 101407, China

E-mail: guoqiang@synfuelschina.com.cn (Q. Guo), jfeng-hu@imu.edu.cn (JF. Hu), yyong@sxicc.ac.cn (Y. Yang), haozhang@imu.edu.cn (H. Zhang).

[*] Corresponding author.

Supplementary Material

1. Parameters for analyzing Mössbauer spectrum data

Table S1 Parameters for analyzing Mössbauer spectrum data

Species	Formula	Fe sites	IS/(mm/s)	QS/(mm/s)	H/(T)
Hexagonal Pyrrhotite[1]	$Fe_{1-x}S$	1	0.74	0.01	33.01
		2	0.72	0.02	30.44
		3	0.71	0.02	28.18
		4	0.74	0.01	25.63
Monoclinic Pyrrhotite[2]	Fe_7S_8	1	0.85	-0.04	33.40
		2	0.86	0.08	31.40
		3	0.81	-0.09	27.10
		4a	0.83	0.08	24.40
		4b	0.82	0.17	20.70
Greigite[3]	Fe_3S_4	a	0.66	-	32.70
		b	0.38	-	31.90
Troilite[4]	FeS	-	0.89	-0.14	32.80
Pyrite[5]	FeS_2	-	0.43	0.66	-
Maghemite[6]	γ-Fe_2O_3	x	0.47	-0.01	51.00
		y	0.34	-0.03	48.10
Magnetite[6]	Fe_3O_4	A	0.42	0.06	51.60
		B	0.99	0.89	51.00
α-Fe[7]	Fe	-	0.09	0.04	33.80

2. Methods of Temperature-Programmed Sulfidation in a Slurry Bed

2.1 H_2S Generation During Temperature-Programmed Sulfidation

Temperature-programmed sulfidation of the iron oxide precursor was conducted in a slurry-bed reactor (internal volume: 100 mL) under a continuous H_2 flow, using 20 g of n-tetradecane as the solvent oil. The reactor was purged with H_2 at a flow rate of

500 mL/min for 5 min. The pressure was then adjusted to 5 MPa using a back-pressure regulator, and the H_2 flow rate was set to 200 mL/min. The temperature was increased to 80 °C at 4 °C/min, followed by a further increase to 350 °C at 1 °C/min. The H_2S content in the tail gas during sulfidation was analyzed online using an Agilent 7890A gas chromatograph.

2.2 Low-Temperature Sulfidation

Low-temperature sulfidation was performed in a slurry-bed reactor (internal volume: 100 mL) under a continuous flow of N_2 or H_2. The reactor was charged with 2 g of γ-Fe_2O_3, 2 g of elemental sulfur ($(S/Fe)_{atom}$ = 2.5), and 20 g of solvent oil (n-tetradecane). It was purged with N_2 or H_2 at 500 mL/min for 5 min. The pressure was adjusted to 5 MPa, and the N_2 or H_2 flow rate was set to 200 mL/min. The temperature was increased to 80 °C at 4 °C/min, then further raised to the target temperature (150 °C, 160 °C, or 170 °C) at 1 °C/min. After reaching the target temperature, the reactor was rapidly cooled to room temperature. The solid catalyst was separated, washed with CS_2, thoroughly rinsed with n-hexane, and then dried in a tubular furnace under N_2 flow (set at 100 °C for 1 h). The dried sample was sealed in a quartz tube and transferred to a dedicated glovebox for XPS analysis. XPS analysis was conducted on an ESCALAB 250xi spectrometer (Thermo Fisher Scientific, USA) equipped with an Al-Kα X-ray source.

3. Temperature-Programmed Sulfidation in a Tubular Furnace

Approximately 50 mg of γ-Fe_2O_3 and 50 mg of elemental sulfur (either together or separately) were placed at the central temperature-measuring point of a quartz tube (6 mm × 3 mm × 100 mm). After confirming system airtightness, H_2 or N_2 was introduced to purge the air inside. Following complete purging, the temperature was held at 50 °C for 1 h. Subsequently, the temperature was increased to 300 °C at a heating rate of 1 °C/min. The concentrations of H_2S and SO_2 in the tail gas were monitored using a Pfeiffer Omnistar™ gas analysis mass spectrometer.

4. The GC results of the post-reaction solution

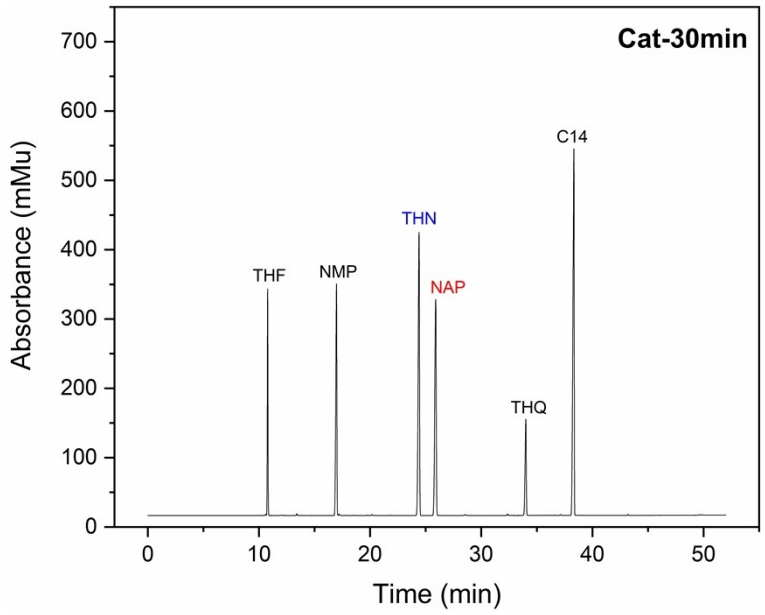

Fig. S1 The GC results of the post-reaction solution following the application of Cat-30min.

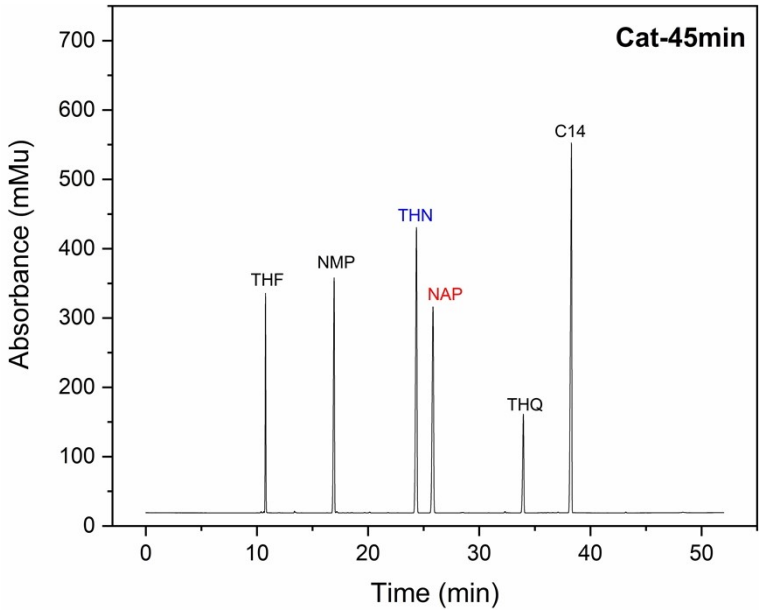

Fig. S2 The GC results of the post-reaction solution following the application of Cat-45min.

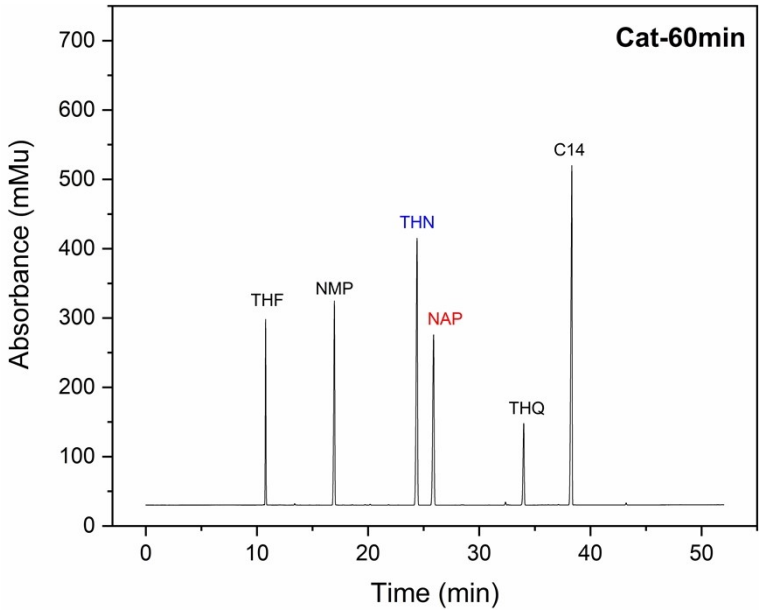

Fig. S3 The GC results of the post-reaction solution following the application of Cat-60min.

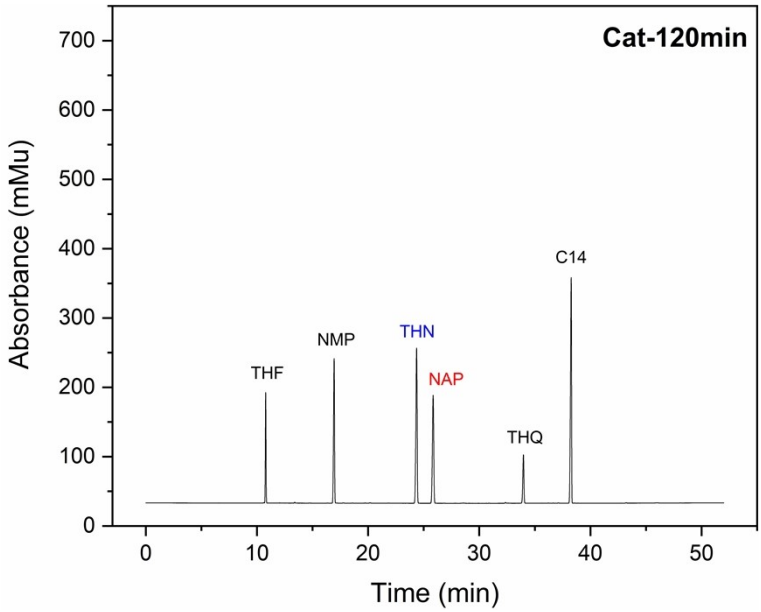

Fig. S4 The GC results of the post-reaction solution following the application of Cat-120min.

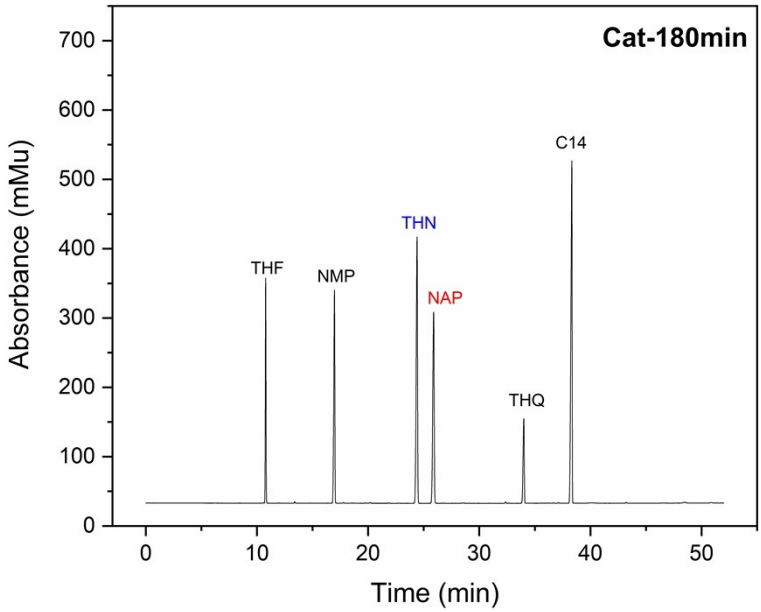

Fig. S5 The GC results of the post-reaction solution following the application of Cat-180min.

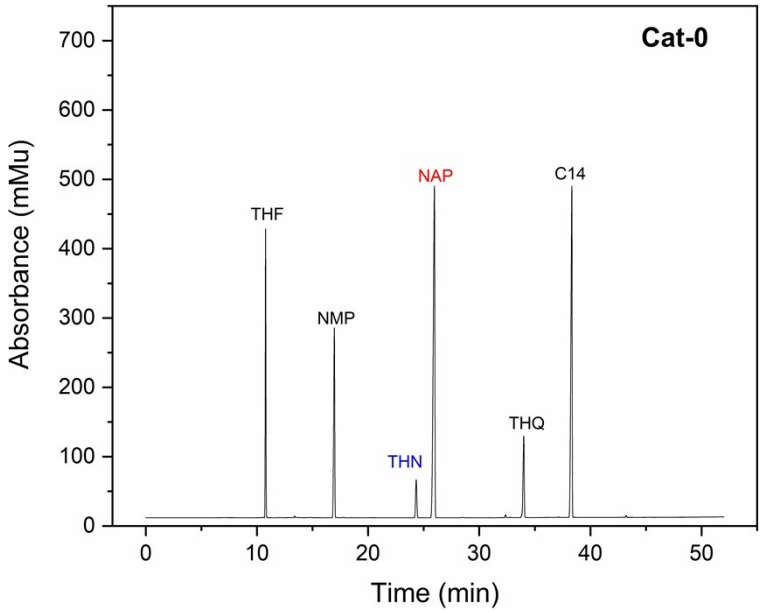

Fig. S6 The GC results of the post-reaction solution following the application of Cat-0.

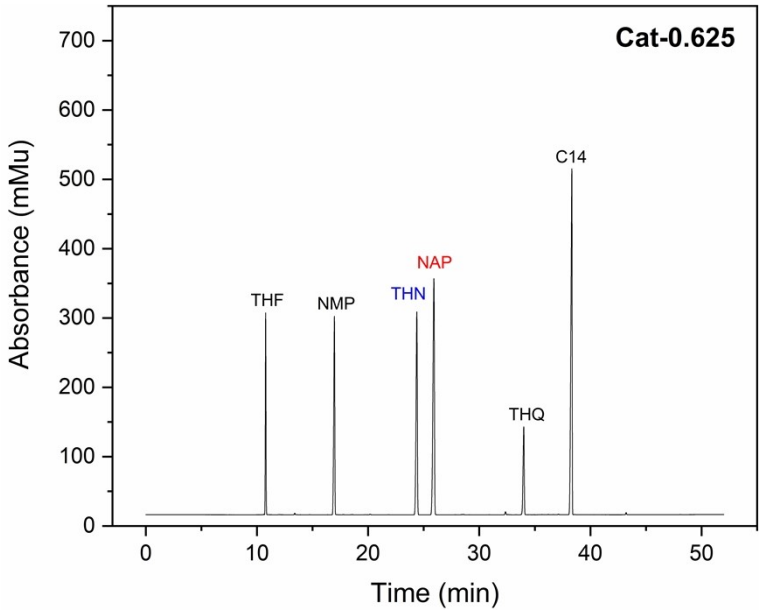

Fig. S7 The GC results of the post-reaction solution following the application of Cat-0.625.

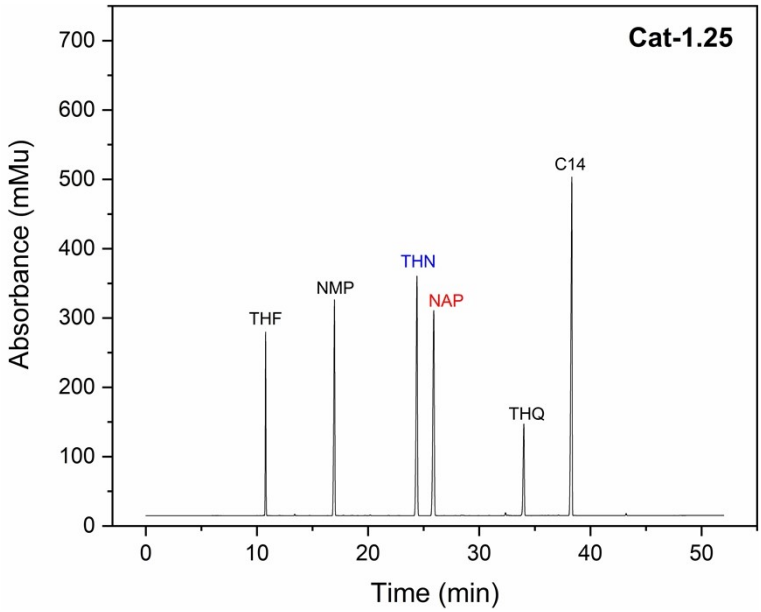

Fig. S8 The GC results of the post-reaction solution following the application of Cat-1.25.

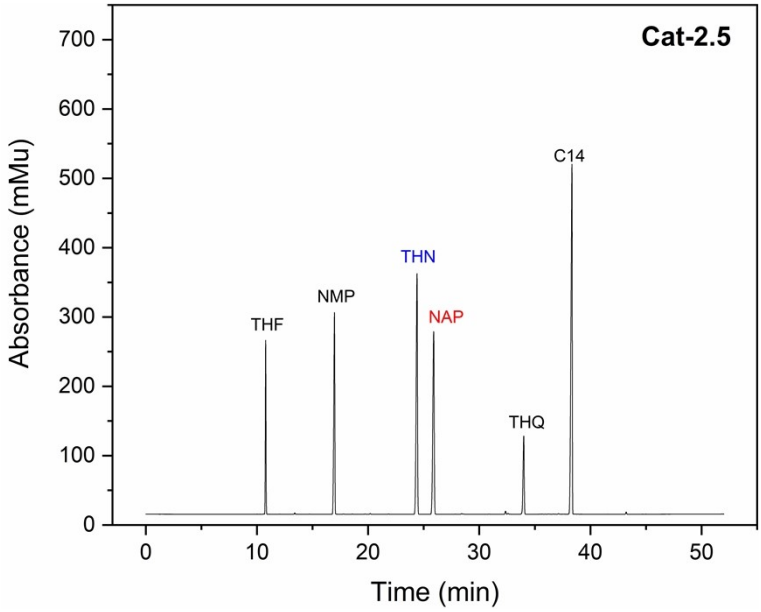

Fig. S9 The GC results of the post-reaction solution following the application of Cat-2.5.

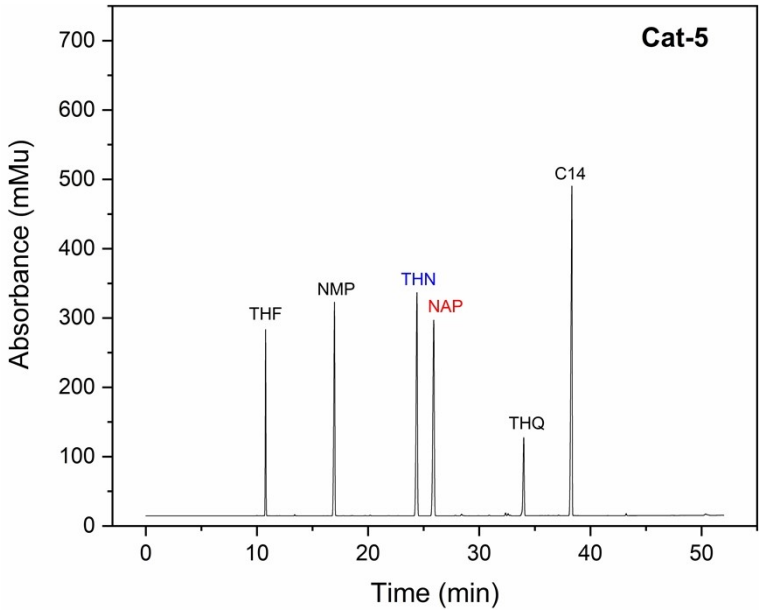

Fig. S10 The GC results of the post-reaction solution following the application of Cat-5.

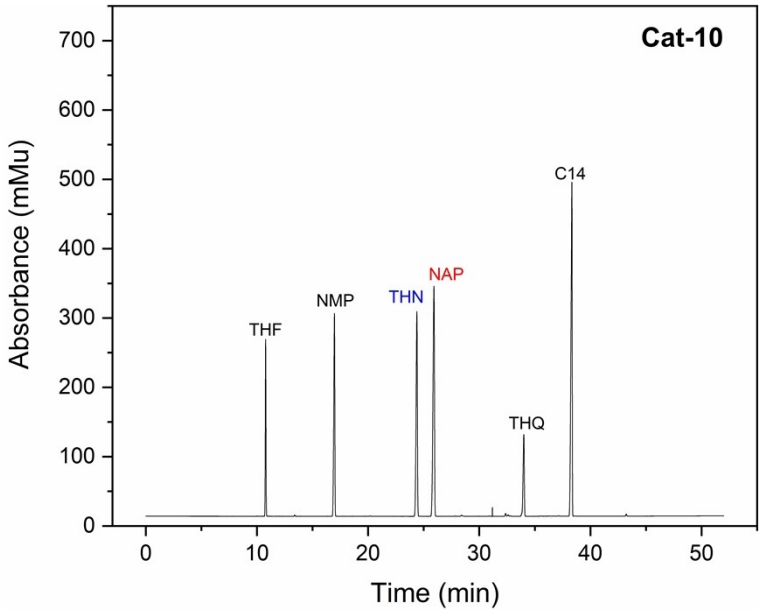

Fig. S11 The GC results of the post-reaction solution following the application of Cat-10.

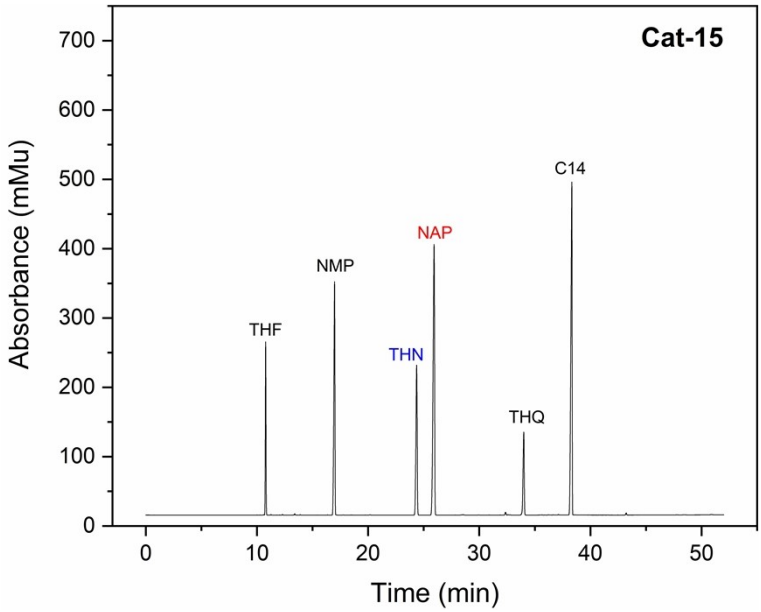

Fig. S12 The GC results of the post-reaction solution following the application of Cat-15.

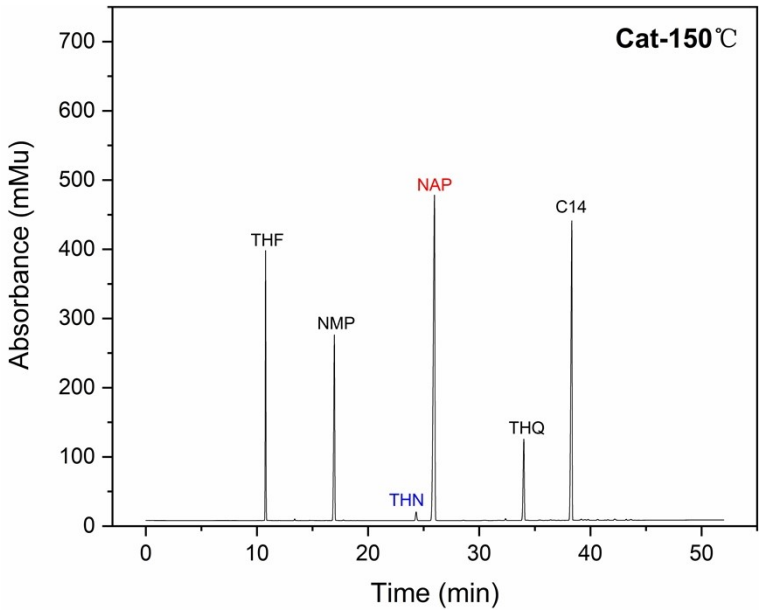

Fig. S13 GC results of the post-reaction solution following the application of Cat-150°C.

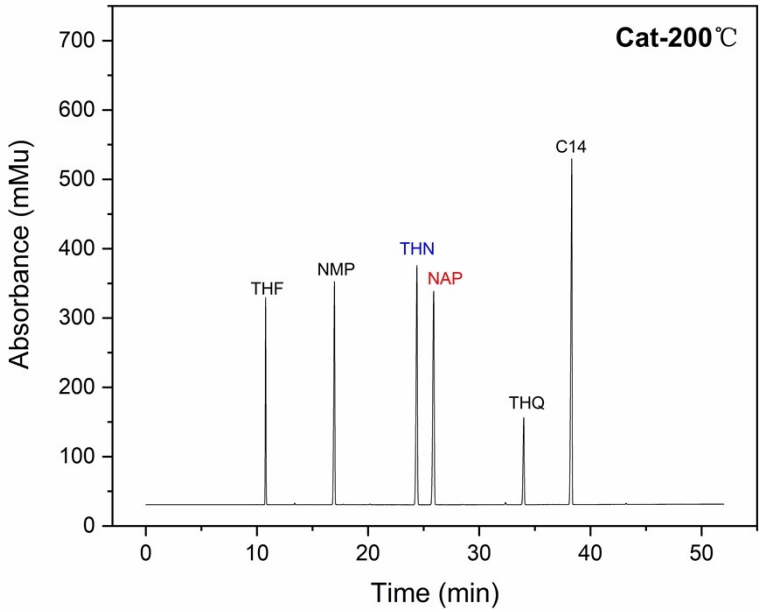

Fig. S14 The GC results of the post-reaction solution following the application of Cat-200°C.

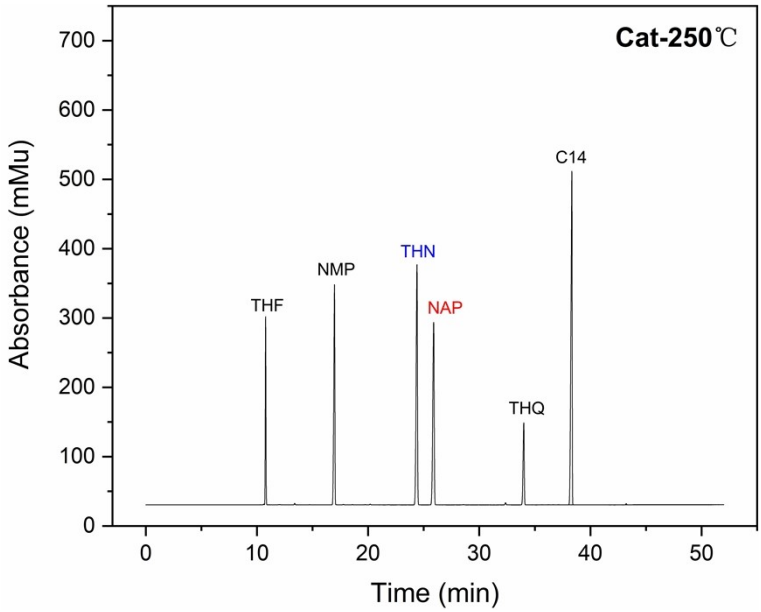

Fig. S15 The GC results of the post-reaction solution following the application of Cat-250°C.

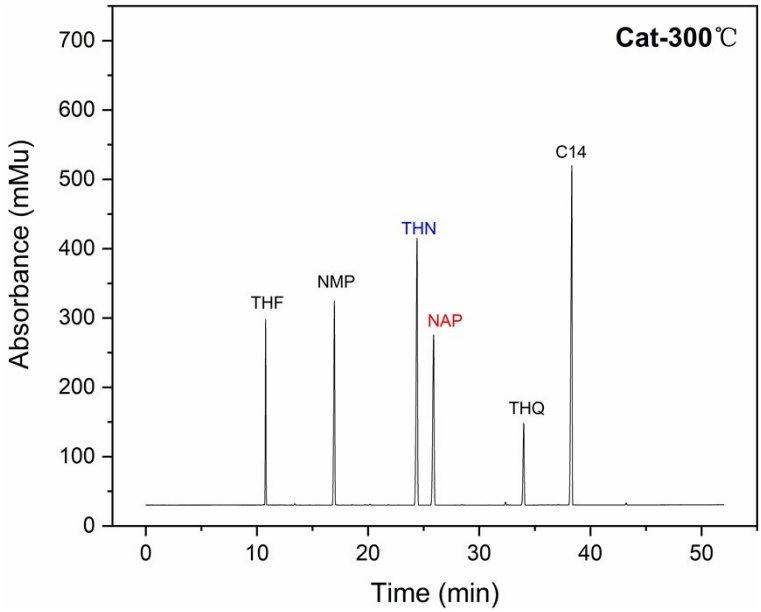

Fig. S16 The GC results of the post-reaction solution following the application of Cat-300°C.

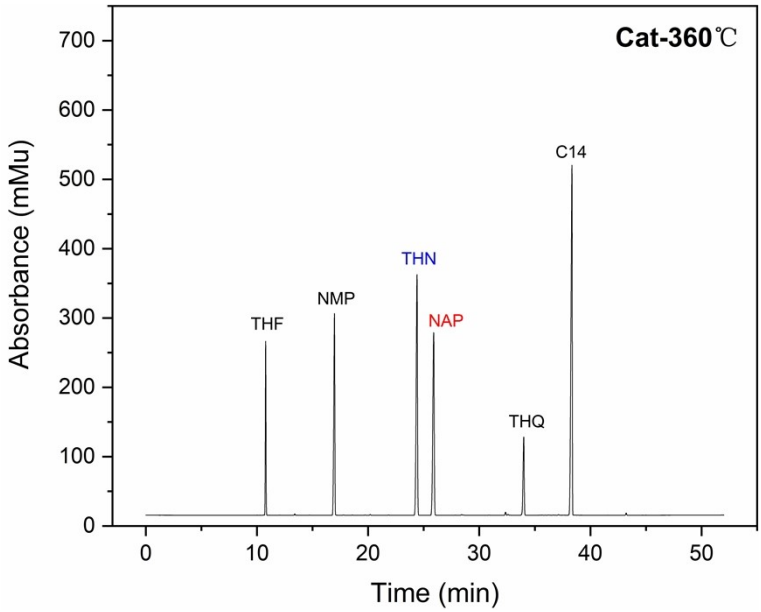

Fig. S17 The GC results of the post-reaction solution following the application of Cat-360°C.

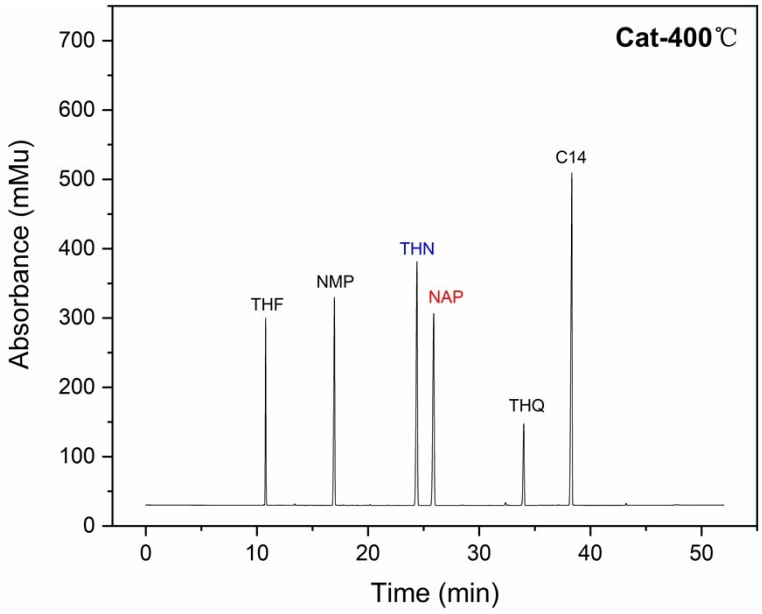

Fig. S18 The GC results of the post-reaction solution following the application of Cat-400°C.

References

1. Kondoro, J. W. A., Mössbauer study of vacancies in natural pyrrhotite. Journal of Alloys and Compounds 1999, 289 (1), 36-41.

2. Jeandey, C.; Oddou, J. L.; Mattei, J. L.; Fillion, G., Mössbauer investigation of the pyrrhotite at low temperature. Solid State Communications 1991, 78 (3), 195-198.

3. Chang, L.; Roberts, A. P.; Tang, Y.; Rainford, B. D.; Muxworthy, A. R.; Chen, Q., Fundamental magnetic parameters from pure synthetic greigite (Fe3S4). Journal of Geophysical Research: Solid Earth 2008, 113 (B6).

4. J. Cuda, T. Kohout, J. Tucek, J. Filip, O. Malina, M. Krizek, R. Zboril, In-field 57Fe Mössbauer spectroscopy below spin-flop transition in powdered troilite (FeS) mineral, AIP Conference Proceedings, 2014, pp. 8-11.

5. P.A. Montano, M.S. Seehra, Magnetism of iron pyrite (FeS2) — a Mössbauer study in an external magnetic field, Solid State Communications 20(9) (1976) 897-898. https://doi.org/10.1016/0038-1098(76)91300-4.

6. S.J. Oh, D.C. Cook, H.E. Townsend, Characterization of Iron Oxides Commonly Formed as Corrosion Products on Steel Hyperfine Interactions 112(1/4) (1998) 59-66. https://doi.org/10.1023/a:1011076308501.

7. I. Kubono, N. Nishida, Y. Kobayashi, Y. Yamada, Mössbauer spectra of iron (III) sulfide particles, Hyperfine Interactions 238(1) (2017). https://doi.org/10.1007/s10751-017-1465-z.